Challenges and Solutions for Ultrasonic Phased-Array Inspection of Polymer-Matrix Composites at Production Rates

Deborah Hopkins[1,a)], Marvin Datuin[1,b)], Michel Brassard[2,c)]

[1]*BERCLI Corp, Berkeley, CA 94703*
[2]*TD NDE, Vaudreuil Dorion, Québec, J7V 5V5 Canada*

a) Corresponding author: deborah@bercli.net
b) marvin@bercli.net
c) mbrassard@tdnde.com

Abstract. More than ten years of Research and Development focused on phased-array inspection of aerospace Polymer Matrix Composites (PMCs) is presented. This work includes basic research designed to understand the propagation of ultrasound through composite materials, as well as optimization of phased-array probes and inspection strategies for composite parts. Successful implementations of these strategies for fully automated on-line inspections are presented including a discussion of how challenges were overcome and the promise of new acquisition and analysis tools. Composite materials present unique challenges for ultrasonic inspection including complex shapes and a wide range of potential flaws and defects. For automated inspections, part-to-part variability and the need to inspect at production rates pose additional challenges. The methodologies presented are based upon laboratory experiments performed in conjunction with modeling and simulations, which are used to optimize inspection strategies. A significant challenge that should not be under estimated is creating industrial-quality test specimens with realistic defects of known size and location that can be independently verified. In projects with industry and the Air Force Research Laboratory (AFRL), work has focused specifically on using surface-adaptive techniques to inspect parts with complex shapes including small convex and concave radii that are typically found on stringers, blades and wing structures. Experimental and simulation results have been evaluated for flat and curved linear arrays as well as matrix arrays, which are used with and without surface-adaptive techniques for purposes of comparison. Fully automated on-line inspections that have been operating for several years as well as recent large-scale implementations demonstrate the ability to inspect a wide range of different composite parts at production rates. Rapidly increasing computer processing power together with ultra-high data-transfer rates will continue to enable computationally intensive signal and image processing in near real time. These advancements hold promise for greater use of automated inspection and the ability to incorporate sophisticated data acquisition and analysis tools into portable systems that can then be used in the field, for example, in depots and onboard ships.

INTRODUCTION

For more than ten years, BERCLI and TD NDE have been actively engaged in research, development and implementation of phased-array inspection methodologies for PMCs [1]. This work has included probe and inspection optimization for a variety of composite parts and applications (see Fig.1). Of the many inspection challenges with composites, complex geometry is perhaps the most difficult, including changes in shape and thickness across the part and small radii. These conditions can make it challenging to obtain full coverage, either because it is difficult to reach certain regions or because back-wall and defect reflections occur at angles that do not make it back to the probe. The need to find solutions for inspecting complex shapes and small radii led to significant efforts in evaluating and implementing surface-adaptive ultrasound (SAUL), described in the following section [2-3]. SAUL is now being used for fully automated inspection of hundreds of composite aerospace parts, which is discussed in the last section.
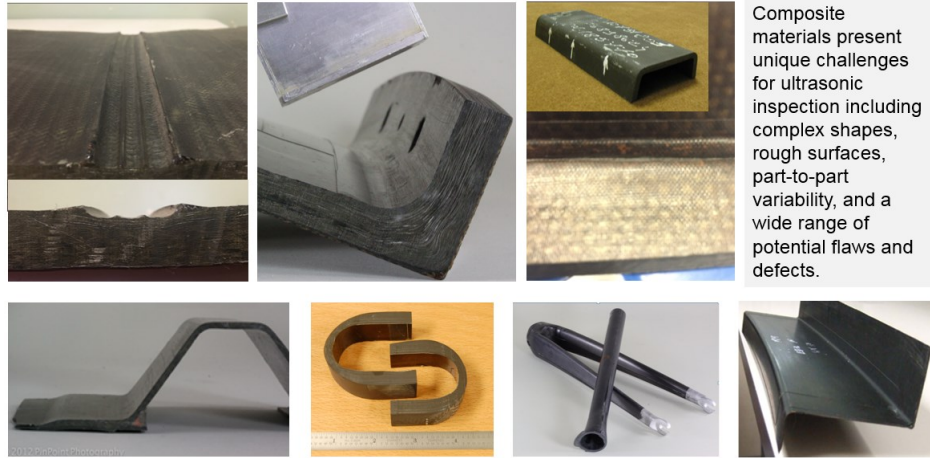
FIGURE 1. Photographs of composite test specimens that encompass the range of parts that have been evaluated in collaboration with industry and government partners.

In optimizing probes and inspection strategies for composite applications there are a large number of options and associated variables that all play a role in determining viable and optimized inspection solutions. Some of the key material, structural, and defect variables are listed in Table 1, along with probe, beam-forming, and inspection variables. In addition, cost, speed, ease of use, and suitability for automation and integration with plant operations must all be concurrently evaluated for industrial applications. The sheer number of factors to be considered makes it cost prohibitive to perform the experiments that would be required to optimize probes and inspection strategies, as well as test and evaluate emerging data-acquisition and signal-processing tools. The approach taken for the work summarized here is to perform simulations and experiments in parallel for design and optimization, as well as for troubleshooting and analyzing data.

Most of the results presented here are from Phases I and II of a Small Business Innovation Research (SBIR) Grant from the Air Force Research Laboratory (AFRL) focused on inspection of leading edges (convex radii) on composite aerospace structures. The parts that have been tested and modeled as part of this project include specially fabricated samples with embedded defects and a variety of actual parts manufactured by suppliers to aerospace primes. The most recent results are focused on evaluating sizing capabilities. The probes and inspection strategies explored build upon previous work and the lessons learned from industrial implementations.

Table 1. Material and inspection variables that impact the design and implementation of optimized inspection strategies

Material Properties and Structure	Resin and fiber material properties; Chopped vs. continuous fibers; Number of plies and structure of layers; Manufacturing and curing processes.
Specimen	Overall size and shape; Thickness; Local geometry; Areas of ply dropoff; Small radii.
Defects	Delaminations; Foreign debris; Impact damage; Porosity; Bridging; Wrinkles /waviness.
Probe	Frequency; Pitch (center-to-center spacing between elements); Number of elements; Size and shape of elements; Spatial arrangement of elements (e.g., linear, matrix, annular); Probe shape (e.g., flat, shaped).
Beam Forming	Number of elements active for each shot; Focusing; Steering.
Inspection	Water path; Scan plan including step size for mechanical and/or electronic scanning; Part following vs. raster scan; Gates and gains applied.

SURFACE-ADAPTIVE ULTRASOUND (SAUL)

The objective of surface-adaptive techniques is to enable inspection of complex geometry and to ease interpretation of the resulting data by producing shape-corrected scans. As mentioned above, in many cases of complex geometry defects cannot be detected because back-wall and defect reflections do not make it back to the probe. In these cases, SAUL's ability to apply delay laws to provide a normally incident wave allows detection of defects not otherwise visible. SAUL was developed at the *Commissariat à l'énergie atomique et aux énergies alternatives* (CEA) in France and patented in 2011 [4-5]. It was implemented in M2M's fully parallel phased-array systems, and subsequently

incorporated into the CIVA 16 simulation platform. Because the phased-array measurement system and CIVA use the same algorithm (except for possible differences in versions) measurements and simulations can be calibrated, compared, and used to explore a much larger range of variables than could be done with experiments alone.

M2M's SAUL is an iterative process [3]. The first step is to fire all of the probe's elements simultaneously to create a full-array plane wave. The signals reflected off the front surface are recorded in parallel for each individual element, providing a measurement of the surface geometry. The time-of-flight to the front surface for each element is used to generate delay laws that are then applied in transmission to obtain a shape-corrected incident wave that is normal to the part across a specified aperture. The iterative algorithm typically converges within 3 shots per position. A reception delay law can also be applied to synchronize the signals measured by individual elements and to create coherent summations of signals obtained via electronic scanning of a sub-aperture.

## SPECIALLY FABRICATED COMPOSITE LEADING-EDGE TEST SPECIMENS

BERCLI and SBIR partner Texas Research Institute (TRI) both fabricated composite test specimens. TRI modeled theirs on an actual empennage part (tail assembly), whereas BERCLI fabricated small-radii test specimens that were tested in conjunction with industry parts to evaluate localization and sizing capabilities using surface-adaptive acquisition. In the sense that the empennage has a relatively large radius it is easier to inspect than the smaller parts with tight radii. The empennage is however very thin, which can be challenging if reflections off defects are convolved with signals reflected off the front and back walls. Results obtained for the empennage sample are not presented here.

Test specimens with realistic defects of known size and location that span the conditions found in practice and that can be independently verified are essential for analyzing detection, localization and sizing capabilities, as well as for calibration, benchmarking and verification/validation studies. The significant challenges in creating these samples include the complexity of the material, the difficulty of purchasing small lots of aerospace composite prepreg, the difficulty of fully controlling each step in the fabrication process, the tendency of embedded defects to move during fabrication, the high likelihood of creating unintended defects, the extreme difficulty of creating multiple identical specimens, and last but not least, the difficulty of achieving the quality of industrial composite parts, with respect to porosity, homogeneity and signal-to-noise ratios. The fabrication challenges are particularly difficult for small parts where radii can be as small as 4 mm (0.16 inches).

The material used for the test specimens discussed in this section is a unidirectional prepreg with 32 plies. The samples were designed to include defect materials used most often in industry: brass inserts were embedded as surrogates for delaminations, and graphoil, poly-release film, and pressure-sensitive tape were used to represent foreign debris. The size of the inserts is 2.54 x 6.35 mm (0.10 x 0.25 ins). Inserts were placed at three depths: two plies from the top and bottom surfaces and mid laminate. At each depth, three inserts were placed to span the radius and a fourth was placed in the flat "web" area (Fig. 2). The plan called for a more closed angle than the 90 degrees shown in the CAD drawing in Fig. 2, but fabrication issues made it impractical given time and budget constraints. BERCLI contracted with a company that specializes in the fabrication of composite parts for DOD aerospace applications. Although very experienced, the challenges listed above all arose as issues. After three test runs, the finalized fabrication process is illustrated in the photographs in Fig. 3. After placement of the inserts, the prepreg was placed between molds. The parts were wrapped in release ply and then in nonwoven breather material. The wrapped samples were vacuum bagged and cured in an autoclave. The location of the brass inserts was confirmed using radiography. The other inserts were also imaged, but did not show up well in the radiographs.
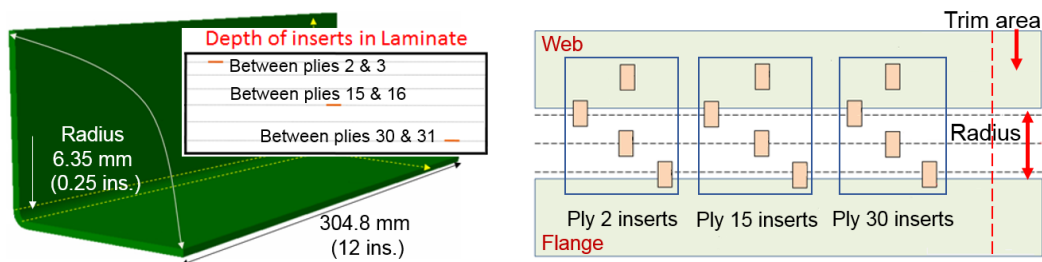

FIGURE 2. Schematic diagrams showing the CAD model for composite test specimens (left-hand image) and the location of embedded inserts at three depths in the laminate. The samples include a trim area that is available for porosity measurements.
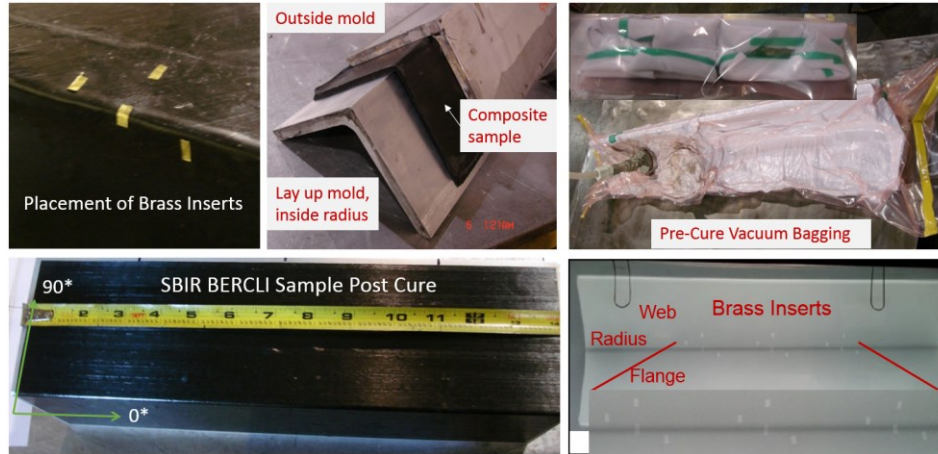
FIGURE 3. Steps in fabricating test specimens with embedded defects: placement of inserts at three depths in the laminate; vacuum bagging and autoclave cure. Radiographic imaging was performed to confirm the location of the brass defects.

The experimental results presented in this section were obtained using an Imasonic 5 MHz 16x4 matrix phased-array probe and an M2M parallel 64-channel controller. The probe was designed and optimized for flexibility so that it would work for a wide selection of parts. A matrix probe was chosen to allow for compensation of geometry in two directions. As described above, all 64 elements are fired simultaneously to obtain the part shape, and for the results in this section, 16-elements (4x4 aperture) are used for reception. Having a relatively large aperture is advantageous for measuring and correcting for the surface shape, whereas using a subset of the probe's elements for reception improves resolution at each measurement location. The optimal reception aperture is something that was studied in detail during Phase II (see Fig. 13). Mechanical scanning in the direction perpendicular to the electronic scan direction allows for C-scans (top view) and B-scans (depth views) in the two scanning directions. The parts were scanned in an immersion tank using a part-following robot. The amplitude C-scan of the web (flat) area is shown in Fig. 4. It appears that the brass inserts at the 3 depths (near front wall, near back wall and mid laminate) were imaged, but the mid-laminate indication is not where it was expected.
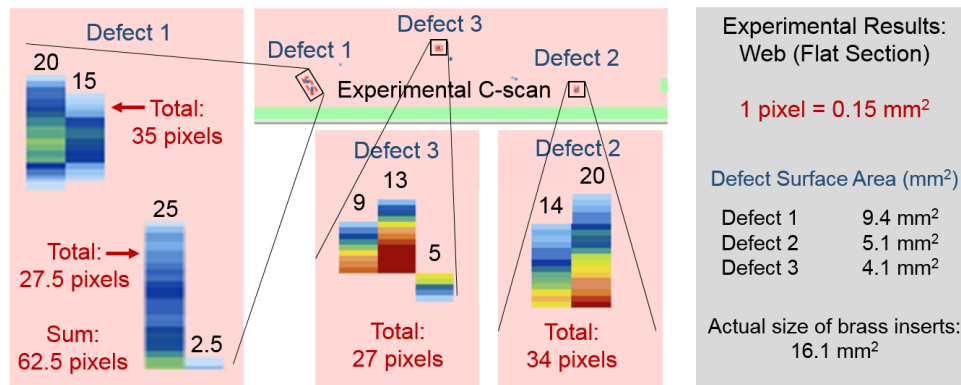
FIGURE 4. Experimental UT results in the web (flat) region of the test specimen with brass inserts (see Fig. 3).

Also shown in Fig. 4 are the estimated sizes of the imaged defects. The acquired experimental data presented here was visualized and analyzed using ULTIS software. The UT images of the defects have been enlarged (exploded views) so that individual pixels are visible. What was identified as Defect 1 consists of two non-contiguous regions. Defects 2 and 3 produced irregularly shaped, but contiguous regions. The surface areas of Defects 1-3 based on pixel count are 9.4, 5.1 and 4.1 mm^2, respectively, compared to the actual size of 16.1 mm^2.

The UT measurements in the radius of the same sample (brass inserts) were obtained using a flat, 16x4, 5-MHz matrix probe with rectangular elements (0.6 x 1.1 mm). No measurements were possible in the radius without the use of SAUL, which is consistent with previous work performed on small radii. The first step in the testing with SAUL is

to optimize the setup to correct for the strong curvature to allow detection and to maximize back-wall signals. The radius amplitude C-scan shown in Fig. 5 indicates that the SAUL reconstruction is working well, based on the strong signals measured in the radius. The areas where no signals are evident indicate internal defects. Once the setup has been optimized, internal gates that do not include the front-surface and back-wall reflections are used to improve the imaging of defects. The C-scan of the radius using an internal gate is shown in Fig. 6. It is believed that defects 2, 4 and 3 are the brass inserts, indicating that the near-surface, mid laminate and back-wall defects were detected and sized. The actual size of the brass inserts is 16.1 mm^2. Defects 1 and 5 are of similar size as the inserts, but are unknown flaws presumably created during fabrication. Additional very small indications are also evident in the radius.
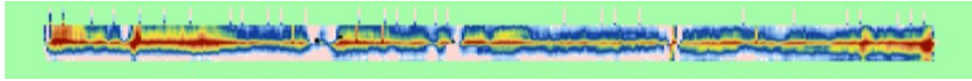

FIGURE 5. Experimental UT results for the convex radius showing that with SAUL good coverage is obtained.
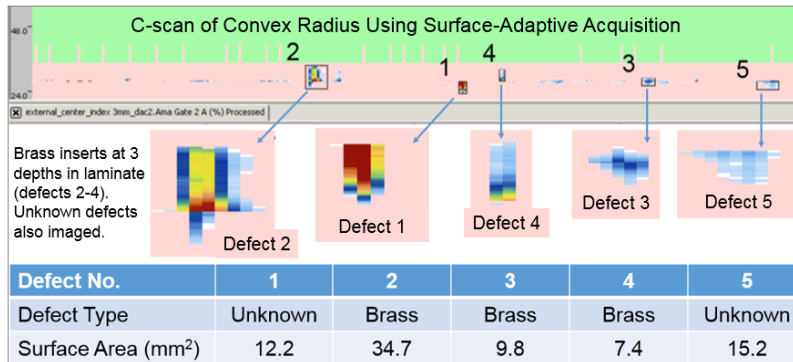

FIGURE 6. Experimental results using an optimized setup for the convex radius including estimated sizes.
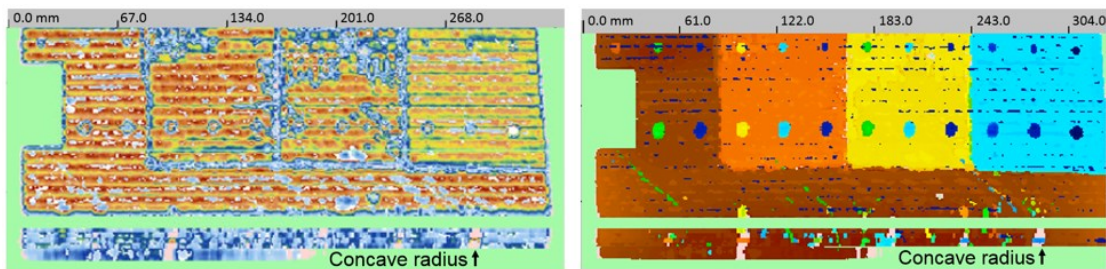
COMPOSITE CALIBRATION BLOCK

A calibration block was machined by drilling flat-bottom holes into an actual aerospace composite part. A photograph of the part post drilling, along with three views of the CAD model showing the hole sizes, are shown in Fig. 7. As can be seen in the photograph, the flat section was machined to create three steps with different thicknesses. The first step in the picture (Step 1) was unchanged and has a thickness of 6.2 mm. After machining, the following three steps have thicknesses of 4.8, 3.8 and 1.8 mm, respectively. Although flat-bottom holes do not mimic the acoustic behavior of delaminations or debris, the objective is to allow detection and sizing resolution to be evaluated, as well as the initial comparisons of simulated and measured UT data. The holes in the flat sections also provide baseline measurements for purposes of comparison to measurements in the radii, and also to study the role of part thickness and hole depth on localization and sizing. These comparisons were not possible with the test specimens created in Phase 1 because there was too much unintended variability in the location and size of delaminations and debris, as well as unplanned defects that were induced in the parts during fabrication. In most cases, comparisons of actual and UT-measured sizes on industrial aerospace parts are not possible either because little if any information is available on the defects induced during manufacturing, and defect locations are not controlled so it is impossible to cover the range of thicknesses, structures, and curvatures necessary to quantify detection, localization and sizing capabilities.

UT amplitude and Time-of-Flight (TOF) C-scans obtained using SAUL with a 12-element aperture and 5-MHz matrix probe with no focusing are shown in Fig. 8. The scans were performed with a 25-mm water path, and step sizes of 1 and 7 elements in the *x* and *y* directions, respectively. The measured longitudinal velocities are 1480 m/sec in water and 3040 m/sec in the carbon-composite part. As indicated in the figure, the concave radius was scanned separately because the scan plan and settings are different for this section. The scans show that good coverage was obtained using SAUL, but the holes are only clearly evident in the TOF scan in the flat sections. The holes in the concave radius are not visible, and only a few holes are visible in the amplitude C-scans. The reason that the holes are not more visible is because the same acquisition gate and gain were used; because of the changes in thickness an important step in designing the inspection is to optimize the gates and gain applied to the signal for each region of the part where there are changes in thickness or geometry. For tight radii it is important to add gain; 3 to 4 dB is typical.
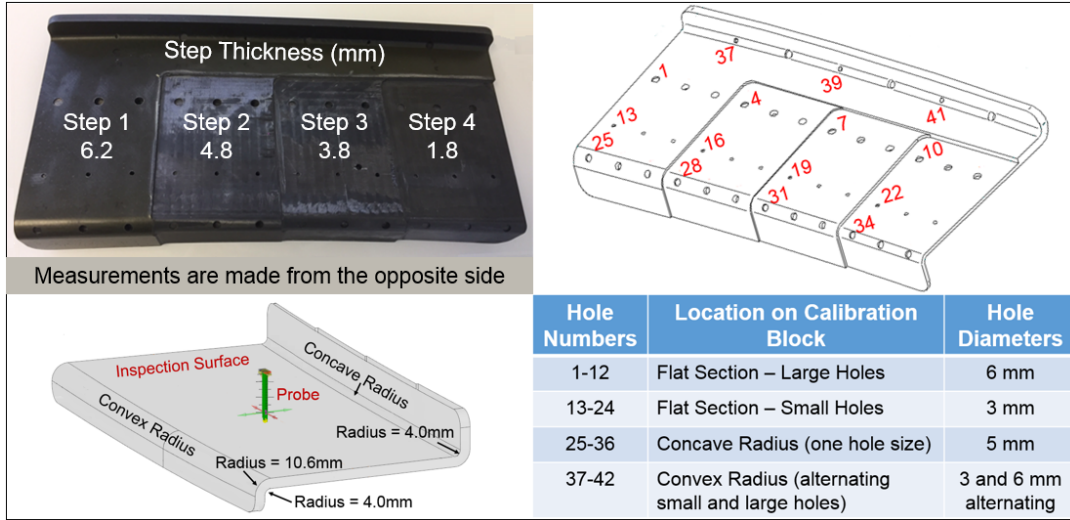
FIGURE 7. Photograph (top left) of calibration block showing how the part was machined to obtain four steps with different thicknesses. In each step, six flat-bottom holes (FBHs) with diameters` of 3 and 6 mm were drilled into the specimen to different depths (hole depths are displayed in the second row of Fig. 9). UT measurements were made from the opposite side (bottom-left image). Hole numbers and locations are shown in the top-right image. Hole diameters are listed in the bottom-right table. For the inspection surface, the holes in the concave radius are 5 mm in diameter; the convex-radius hole diameters alternate between 3 and 6 mm.


FIGURE 8. Amplitude C-scan (left-hand image) and time-of-flight C-scan (right-hand image) for UT measurements on the composite calibration block for a SAUL aperture of 12 elements, with no focusing and a 25 mm water path. The top images in each panel are scans of the flat sections. The concave radius was measured separately so that the scan plan and gates could be optimized for each region, but the gates were not optimized for imaging the holes.

Experimental and simulation results for the flat sections of the calibration block are shown in Fig. 9. The images in the first two rows show the hole pattern in the flat regions and the hole depths. In contrast to the amplitude C-scan in Fig. 8, the amplitude C-scan for the UT measurements of the flat sections shown in Fig. 9 (row 3) clearly show both the large and small holes. In this case, internal gates have been applied for each region that exclude the front-wall and back-wall reflections, thereby enhancing the hole indications. The experimental results are followed by simulated C-scans for the same sections for 5-MHz linear and matrix arrays used with and without SAUL. The simulations were performed in CIVA 16. For the linear probe, scans were performed using 4 active elements, and for the matrix probe a 16-element (4x4) active aperture was used. In both cases, a combination of electronic and mechanical scanning were used to cover the part. In general, the best results achieved to date for composite parts have been obtained using a matrix probe, particularly for concave radii, convex leading edges, and complex shapes. In this case however the simulations show excellent results with the linear probe because the part is flat in this region. If acceptable results can be achieved with a linear probe then it is a desirable solution because linear probes are much less expensive than matrix arrays and fewer channels are required for the phased-array system, which also translates into a cost savings.

The estimated hole sizes based on the diameter of the simulated and measured data are shown as bar charts in Fig. 10. The horizontal black lines in the graphs represent the actual size of the holes (confirmed via CMM). As discussed above, it is important to note that the two data sets are not directly comparable because in both cases the sizes are estimated from the UT images, which is particularly difficult for the experimental data.
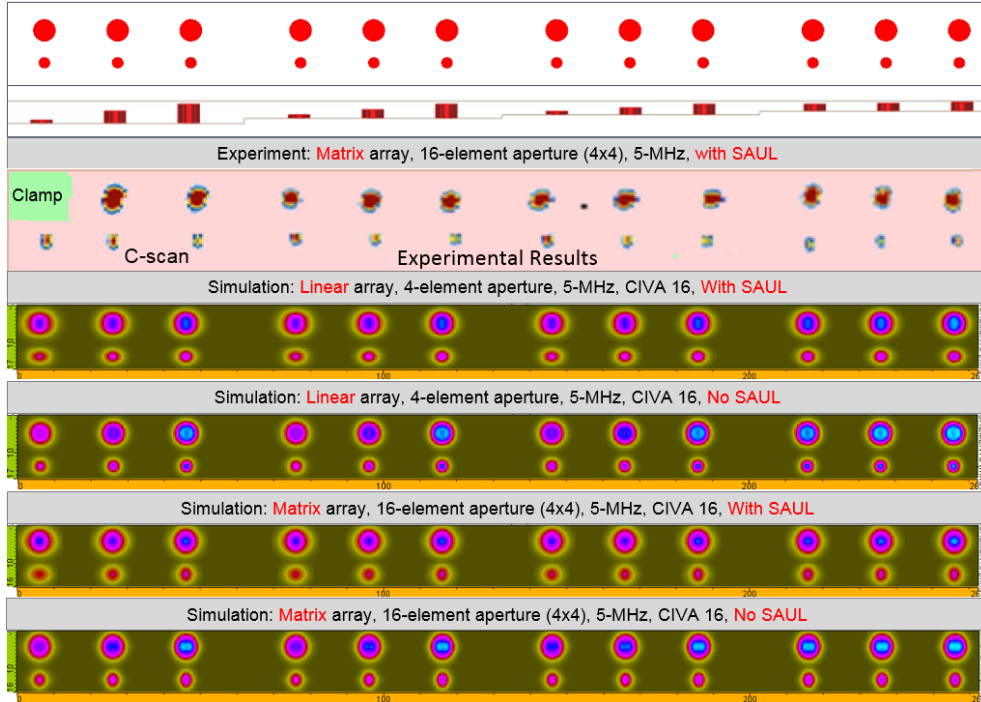
FIGURE 9. Simulation results are shown for the flat section of the composite calibration block to allow simulation and experimental results to be compared with respect to detection, sizing resolution, and relative signal amplitudes. The results shown here are for 5 MHz linear and matrix probes with 4 elements active (linear) and a 16-element aperture (4x4) for the matrix probe. The indications were sized and are compared in Fig. 10.
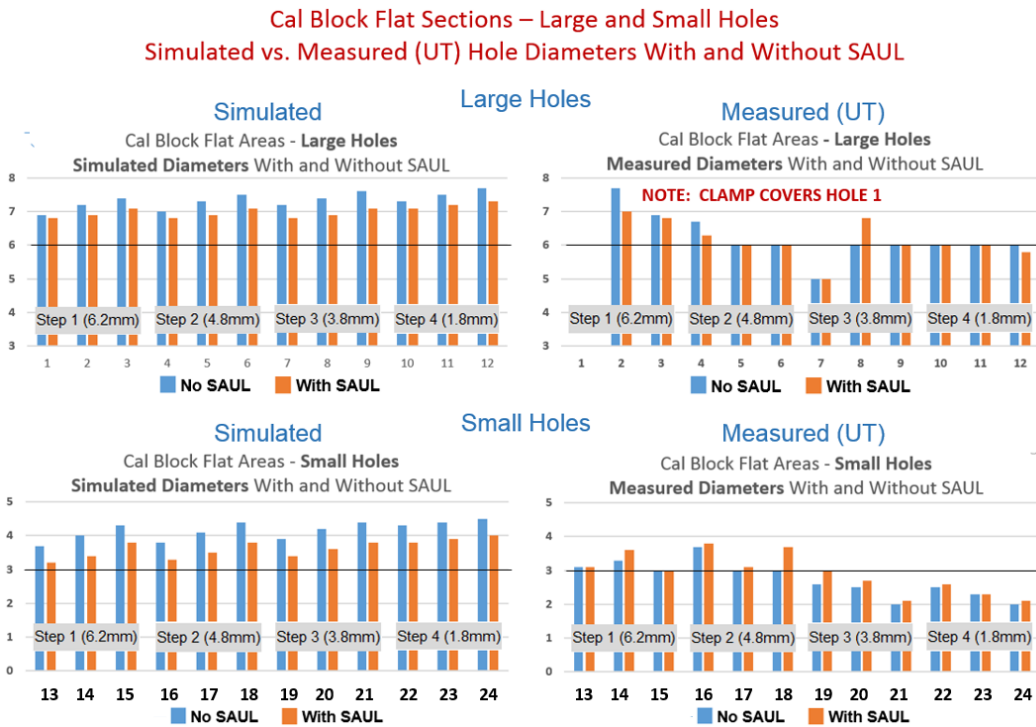

FIGURE 10. Holes sizes (diameters) are compared for simulated (left-hand side) versus measured UT images (right-hand side) obtained with and without SAUL (orange versus blue bars, respectively). The black horizontal lines in the charts indicate the actual hole sizes of 3 and 6 mm (confirmed by CMM measurements).

In comparing the estimated sizes in Fig. 10, it is important to note that the indications in the measured UT data were sized by overlaying a circle (by eye) based on signal amplitude. The indications in the simulated data were sized based on a dB drop in amplitude, indicated by a color scale that was also identified by eye. Additionally, tweaks to the experimental setup were made to optimize the return signals and these modifications are not accounted for in the simulations. It makes most sense therefore to compare the general trends in the sizing data and not the diameter sizes.

For the large holes, the experimental UT measurements in Fig. 10 are generally closer to the actual sizes than the simulated data with the notable exception of Hole 7, for which no explanation is apparent thus far. For the simulations, for the large and small holes, both the no-SAUL and SAUL data over estimate the hole size, and the over estimation is greater for the no-SAUL case. Again for all cases in the simulated data, the estimated diameter of the three holes in each step increase with decreasing depth in the step. The overestimation also increases as the thickness of the step decreases, presumably due in part to more of the reflected energy returning to the probe. These trends are not seen in the measured UT data, where the estimated diameters are smaller than the simulated sizes and where the no-SAUL and SAUL results are very close (with three exceptions). An interesting feature in the UT data that is also in contrast to the simulated data is that with one exception, the estimated diameters for both large and small holes depend on the step thickness, with sizes that are greater than or equal to the hole size for the two thickest steps, and less than or equal to the true size for the two thinnest steps.

For the 6 FBHs in the convex radius displayed in schematic diagrams in Fig. 11, results from experiments and simulations are compared in Fig. 12. The top image (12a) shows the experimental C-scan for the convex radius. The highest amplitude pixels are identified by eye in ULTIS, as indicated by the black circles, which are then measured. The following two images (12b-12c) are identical simulation results obtained using SAUL, also with a 12-element aperture so that the experimental and simulated images are comparable in that sense. The black circles shown in the first simulated image (12b) correspond to the actual hole sizes based on the CAD file for the part. The circles are overlain on the C-scan automatically in CIVA and are not always symmetric with respect to the UT image of the hole. The second simulated image (12c) shows the estimated sizes of the indications in the image that are determined by eye using a built-in measurement tool. As discussed above, the estimated sizes in the simulation images were done independently with no attempt to develop a sizing methodology to obtain a best fit to the experiments.
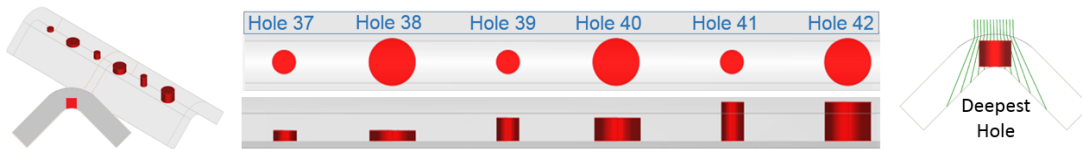
FIGURE 11. CAD model of the calibration block including the flat-bottom holes that were drilled into the convex radius (left-hand image). Top and side views of the holes are shown in the middle image. The right-hand image shows the side view of the test specimen. The green lines show the simulated beam entering the part and the beam paths in the sample.
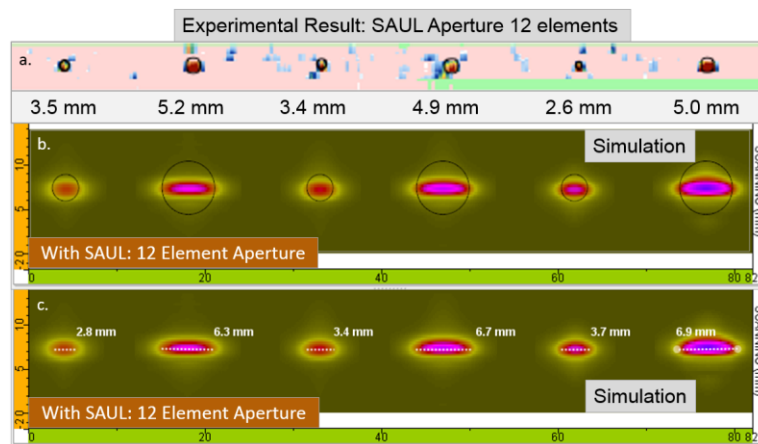

FIGURE 12. The top image (11a) shows the experimental C-scan for the convex radius measured using SAUL with a 12-element aperture. The estimated diameters are displayed below the image. The following two images show the same simulated C-scan obtained using SAUL also with a 12-element aperture. In Fig. 11b, black circles indicating the actual hole sizes are overlain on the C-scan. The bottom image (11c) shows the lines that were used to estimate the diameters of the indications.

The simulated results using SAUL for small radii produce an elliptical indication, as can be seen in Fig. 12. Several additional simulation studies have been performed to understand the ellipticity, including the effects of frequency, rectangular vs. square elements, the SAUL reception aperture, the radius of curvature, and electronic vs. mechanical scanning around the radius. Analyzing these results is in progress, but the radius of curvature is one of the key variables because of its impact on the reflected signals that make it back to the probe.

Additional simulations and experiments were performed to study the effect of the SAUL aperture (the number of active elements used for the surface-adaptive algorithm). Results for the radius for apertures of 8, 12, and 16 elements are shown in Fig. 13 with and without SAUL. The estimated sizes of the indications are plotted and compared to the experimentally derived sizes shown in Fig. 13 for the small and large holes. For the experiments, the 8-element aperture gives the best results for the large and small holes compared to other apertures, whereas the 12-element aperture is best for the simulation results. Recall that simulation results were not calibrated to give the best fit to the experimental data, and that no signals were measured for the convex radius without using SAUL.
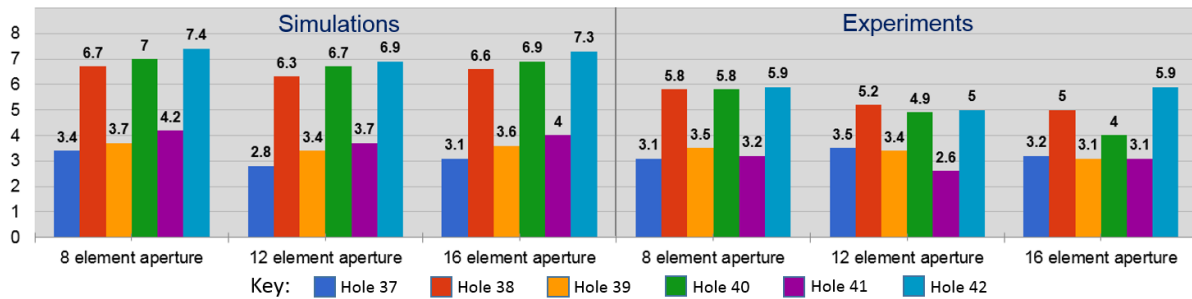
FIGURE 13. Bar charts showing hole diameters estimated from simulations (left-hand side) and experiments (right-hand side) using SAUL for the convex radius for 3 reception apertures (8, 12 and 16 elements). Actual diameters are 3 and 6 mm.

FULLY AUTOMATED INDUSTRIAL IMPLEMENTATIONS

There are two fully automated industrial inspection systems utilizing SAUL that have been implemented at Airbus facilities [6]. The over-riding objective of the project is to integrate state-of-the-art technologies for part handling and inspection to allow rapid evaluation of small complex composite parts. A single flat matrix probe is being used to inspect hundreds of different composite parts similar to the one shown in Fig. 14. The picture shows the inspection setup in the water tank including a five-axis robot. Using SAUL, the average inspection rate for various part geometries in the current ship set is about 120 mm/sec, corresponding to a typical inspection time of 2.5 minutes. This exceeds the required inspection speed of 4 minutes per part. The benefits that have been realized through the use of SAUL are listed in the figure. Emerging techniques used together with SAUL may bestow additional benefits in the future.
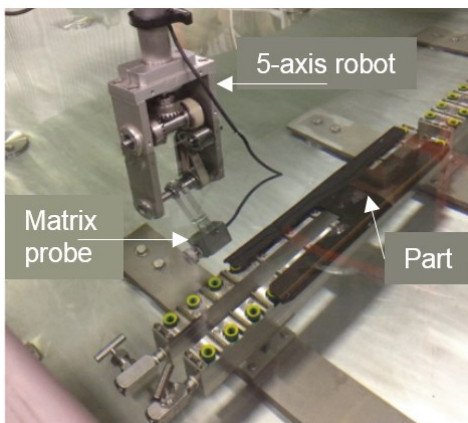
SAUL can impart cost savings while also increasing throughput because it:

- Reduces the number of probes required thereby reducing the cost of the inspection. The ability to use the same probe for a wide variety of parts reduces inventory and eliminates the costs associated with changing probes in and out.
- Greatly reduces the sensitivity of results to probe orientation, thereby greatly improving the accuracy, repeatability, and robustness of the inspection.
- Reduces the challenge of scanning and robot tracking, thereby reducing mechanical complexity and reducing costs.
- Reduces the complexity of the inspection, thereby improving reliability and simplifying data interpretation.

FIGURE 14. Photograph of a composite part undergoing inspection in immersion (left-hand image) and benefits realized using surface-adaptive ultrasound for this fully automated implementation where hundreds of different parts are inspected (right-hand side). Visible in the photograph is the 5-axis cartesian robot holding the 16x4 matrix phased-array probe.

RECOMMENDATIONS FOR FUTURE WORK

Improved localization and sizing, as well as methods to evaluate porosity and characterize sub-surface impact damage are all ways that current composite inspections can be improved. Emerging technologies and signal-processing tools stand to contribute to all of these inspection challenges. Ultra-high data-transfer rates and exponential growth in computer processing power are enabling sophisticated image and signal processing, as well as the use of multiple probes and advanced techniques used in combination, all at production rates [7-8]. But the significant challenges in testing and validating these new methodologies for composite parts should not be under estimated. Similarly, as discussed above, composite test specimens with complex geometry with realistic defects are very difficult to fabricate, especially in matching the quality of production parts with respect to porosity, signal-to-noise ratio and uniformity. Improving sizing means overcoming fabrication issues that make it difficult to embed surrogate defects in specified locations that capture the range of geometries, radii, and thicknesses of aerospace composites. Ensuring a means to independently verify the location of defects post cure is also necessary.

To meet these challenges, basic research is required to better understand material properties including how materials age in practice, the origin of defects and how they respond to changes in stress/strain and material degradation, the propagation of ultrasound in composite materials and complex geometries, and the interaction of ultrasound and defects in realistic geometries. There is also critical information that is application dependent, for example, understanding what defect locations are most critical, how flaws/defects introduced during manufacturing evolve over time, and the mechanical and acoustic interaction of defects and ultrasound in situ.

Benchmarking that allows comparison of simulated and experimental data is always a significant challenge, even for homogeneous materials and idealized defects like side-drilled holes where the mathematics of beam-defect interactions are well understood. Simulations always need to be calibrated, and probably in a more sophisticated way for complex materials like composites compared to traditional engineering materials. Benchmarking experiments and simulations for composites will require significant resources because of the complex materials and structures.

ACKNOWLEDGMENTS

REFERENCES

1. M. Brassard, E. Pelletier, D. Hopkins, G. Neau, S. Robert, "Self-adaptive robotic phased array inspection system for small composite parts of various geometries," Proc., ASNT NDE of Aerospace Materials & Structures III, St. Louis, MO, (2012).
2. D. Hopkins, G. Neau, L. Le Ber, "Advanced phased-array technologies for ultrasonic inspection of complex composite parts," Proc., Smart Materials, Structures, & NDT in Aerospace, NDT in Canada, Montreal (2011).
3. D. Hopkins, L. Le Ber, W. Johnson, G. Neau, "Self-adaptive focusing for phased array inspection of complex composite specimens," Proc., 38th Annual Review of Progress in QNDE, eds. D. E. Chimenti and L. J. Bond, Burlington, VT (2011).
4. S. Mahaut, O. Roy, S. Chatillon, P. Calmon, "Modeling and application of phased array techniques dedicated to complex geometry inspection," Proc., 39th Annual Review of Progress in QNDE, eds. D. E. Chimenti and L. J. Bond, Denver, CO (2012).
5. S. Robert, O. Casula, M. Njiki, O. Roy, "Assessment of real-time techniques for ultrasonic nondestructive testing," Proc., 39th Annual Review of Progress in QNDE, eds. D. E. Chimenti and L. J. Bond, Denver, (2012).
6. M. Brassard, D. Hopkins, J. N. Noiret, "Integration of robotics and surface-adaptive phased-array ultrasound for fully automated inspection of complex composite parts," JEC Composites Magazine, **83**, Aug-Sept 2013, 66-71.
7. D. Hopkins, D. Braconnier, "Transformative technologies and what they mean for inspection," *Quality*, Feb. 2018, NDT Special Section, p. 6A.
8. E. Carcreff, G. Dao, D. Braconnier, "Fast total focusing method for ultrasonic imaging," Proc., 42nd Annual Review of Progress in QNDE," eds. D. E. Chimenti and L. J. Bond, Atlanta, AIP, **1706**, 040001-1 (2016).